

ULTRASONIC DOUBLE BACKSCATTERING IN BETA-FORGED

TI-6AL-4V ALLOY

Yingdong Fu, Xiongbing Li

School of Traffic and Transportation Engineering
Central South University
Changsha, China

Joseph A. Turner

Mechanical and Materials Engineering
University of Nebraska-Lincoln
Lincoln, NE, USA

ABSTRACT

Ultrasonic double backscatter techniques are widely used to evaluate microstructure and detect flaws during high frequency ultrasonic inspections. For typical microstructure of beta-forged Ti-6Al-4V alloy, a new double scattered response (DSR) model that considers the lamellar microstructure within grains and the grain size distribution along the major axis is developed based on a previous DSR model. Numerical results show that the amplitude of ultrasonic scattering decreases because of elongated grains and major axis distribution of grain size. This work is anticipated to play an important role in microstructural characterization research associated with ultrasonic scattering for the beta-forged Ti-6Al-4V alloy.

Keywords: Ultrasonic double-scattering; Beta-forged Ti-6Al-4V alloy; Two-point correlation function, Grain size distribution.

NOMENCLATURE

α	alpha
β	beta
θ	theta
φ	phi

1. INTRODUCTION

Ultrasonic scattering resulting from grain boundaries in polycrystalline materials has a significant negative effect on ultrasonic imaging in medical and nondestructive evaluation applications. However, the scattered signals carry very important information about the sample microstructure and can be used to quantify the length scales associated with grains or intergranular microstructure and detect flaws if properly modeled.

2. MATERIALS AND METHODS

Due to their good comprehensive performance, forged Ti-6Al-4V alloys are widely used in high-end fields including

aerospace and military [1, 2]. According to the different forging temperature, it can be divided into $(\alpha+\beta)$ forging and β forging.

In this work, we focused on the beta-forged Ti-6Al-4V alloy with the typical lamellar microstructure [3].

2.1 Ultrasonic double-scattering model

A time-dependent model of the spatial variance was derived by Hu and Turner [4] to account for both first and second scattering effects. This doubly-scattered response (DSR) model can be expanded as

$$\Phi_{DSR}(t) = \Phi_{LL}(t) + \Phi_{LLL}(t) + \Phi_{LTL}(t), \quad (1)$$

where $\Phi_{LL}(t)$ is the first-order scattering. In fact, $\Phi_{LL}(t)$ is $\Phi_{SSR}(t)$ and is the primary time-dependent spatial variance model under the assumption of a singly-scattered response (SSR) [5]. The DSR is a sum of the SSR and the second-order scattering, $\Phi_{LLL}(t)$ and $\Phi_{LTL}(t)$, that define the longitudinal and transverse components of the second-order scattering, respectively. Generally, the $\Phi_{LL}(t)$, $\Phi_{LLL}(t)$, $\Phi_{LTL}(t)$ can be expressed as

$$\Phi_{LL}(t) = \Phi_{SSR}(t) = \Phi_0 \times \left[\tilde{\eta}_{LL}(\theta_{ps}) \Xi_{\dots \hat{p}_0 \hat{p}_s \hat{s}_0}^{\dots \hat{p}_0 \hat{p}_s \hat{s}_0}(\theta_{ps}) \right] \times \psi_{LL}, \quad (2)$$

$$\Phi_{LLL}(t) = \Phi_0 \times \left[\tilde{\eta}_{LL}(\theta_{ps}) \Xi_{\dots \hat{p}_0 \hat{p}_s \hat{s}_s}^{\dots \hat{p}_0 \hat{p}_s \hat{s}_s}(\theta_{ps}) \right] \times \left[\tilde{\eta}_{LL}(\theta_{sq}) \Xi_{\dots \hat{s}_q \hat{q}_0}^{\dots \hat{s}_q \hat{q}_0}(\theta_{sq}) \right] \times \psi_{LLL}, \quad (3)$$

$$\Phi_{LTL}(t) = \Phi_0 \times \left[\tilde{\eta}_{Lr}(\theta_{ps}) \Xi_{\dots \hat{p}_0 \hat{p}_s \hat{s}}^{\dots \hat{p}_0 \hat{p}_s \hat{s}}(\mathbf{I}_{-\hat{s}})(\theta_{ps}) \right] \times \left[\tilde{\eta}_{Lr}(\theta_{sq}) \Xi_{\dots \hat{s}}^{\dots \hat{s}}(\mathbf{I}_{-\hat{s}})_{\hat{s}_q \hat{q}_0}(\theta_{sq}) \right] \times \psi_{LTL}. \quad (4)$$

where Φ_0 is used to denote a constant related to the experiment calibration. $K_{total}^{uv}(\theta) = \tilde{\eta}_{LL}(\theta_{ps}) \Xi_{\dots \hat{p}_0 \hat{p}_s \hat{s}}^{\dots \hat{p}_0 \hat{p}_s \hat{s}}(\theta_{ps})$ defines the diffuse backscatter coefficient, which is used to quantify the microstructural properties. $\tilde{\eta}_{LL}(\theta_{ps})$ represents the spatial correlation function. $\Xi_{\dots \hat{p}_0 \hat{p}_s \hat{s}}^{\dots \hat{p}_0 \hat{p}_s \hat{s}}(\theta_{ps})$ is the inner product on the

eighth-rank tensor of the covariance of elastic modulus fluctuations [5]. ψ_{LL} is the field distribution function describing the transducer beam and the input pulse.

2.2 Two-point correlation function

The two-point correlation function represents the probability that two randomly chosen positions lie within a region of the material that has uniform properties [6]. When the grain is assumed to be equiaxed, the two-point correlation function can be expressed as [7]

$$W_{equiaxed}(r) = \exp(-r/L), \quad (5)$$

where L is the radius of the mean grain size. When the grains are elongated, we generalize this to the form used by Ahmed and Thompson [8] in the analysis of attenuation

$$W_{elongated}(r) = \exp[-r\{1+(L_a^2/L_c^2-1)\cos^2(\theta)\}^{1/2}/L_a]. \quad (6)$$

Figure 1 shows the geometry of an elongated grain, in which the interpretation of L_a as the grain radius along the y -axis of rotational symmetry and L_c as grain radius in the perpendicular plane is evident.

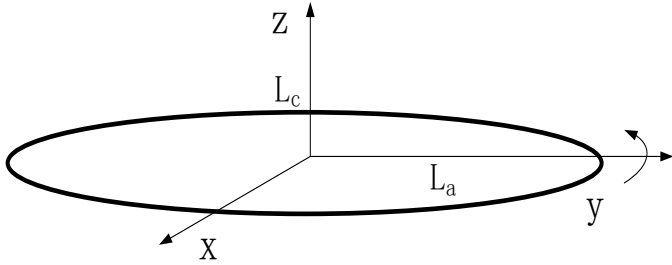


FIGURE 1: SCHEMATIC REPRESENTATION OF ELONGATED GRAIN.

For beta-forged Ti-6Al-4V alloy, the two-point correlation function is modified by considering a distribution of grain sizes.

$$W_{distribution}(r) = \int_0^\infty P(L_a) \exp[-r\{1+(L_a^2/L_c^2-1)\cos^2(\theta)\}^{1/2}/L_a] dL_a, \quad (7)$$

where L_c is constant. $P(L_a)$ is a log-normal distribution function of grain radius along the y -axis of rotational symmetry (L_a). $P(L_a)$ can be written as

$$P(L_a) = \frac{1}{L_a \sigma_d \sqrt{2\pi}} \exp\left(-\frac{\ln^2(L_a/L_a)}{2\sigma_d^2}\right), \quad (8)$$

Where L_a is the median of the distribution given by $L_a = \exp \mu$ which relates to the mean by $\bar{L}_a = L_a \exp(\sigma_d^2/2)$ and to the mode by $L_a^M = L_a \exp(-\sigma_d^2)$. Note that \bar{L}_a is the volumetric mean of the distribution and not the arithmetic mean.

The spatial Fourier transform of the covariance is given by

$$\tilde{\eta}(\mathbf{p}) = \frac{1}{(2\pi)^3} \int d^3r W(r) e^{i\mathbf{p}\cdot\mathbf{r}}, \quad (9)$$

where \mathbf{p} is the wave vector. The general expressions of double scattering from Hu and Turner [4] may then be simplified for the case of beta-forged Ti-6Al-4V materials using the two-point correlation function.

3. RESULTS AND DISCUSSION

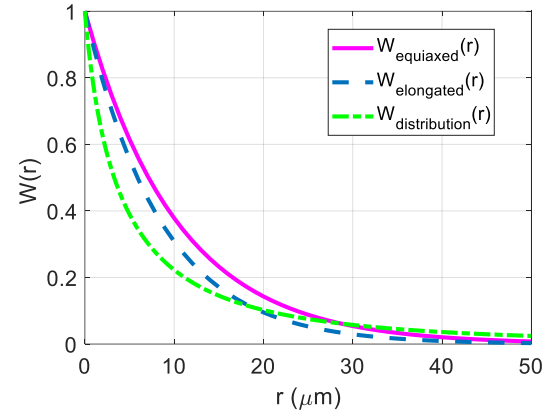


FIGURE 2: (Color online) Comparison of the two-point correlation functions based on the different grain models. $L=10\mu\text{m}$, $L_a=10\mu\text{m}$, $L_c=2\mu\text{m}$.

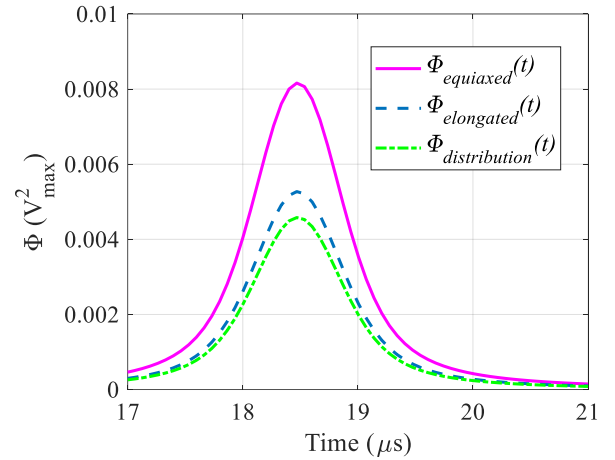


FIGURE 3: (Color online) Comparison among the maximum amplitudes of the DSR models based on the different the two-point correlation functions.

4. CONCLUSION

In this work, the distribution of grain size along the major axis is introduced to modify the doubly-scattered response (DSR) model for beta-forged Ti-6Al-4V alloy. The results show that the modified DSR model can accurately predict the maximum amplitude of backscatter signals induced by the microstructure. In future work, this model will be used to calculate the corresponding bounds of grain noise and finally enhance the ultrasonic detection of small flaws in beta-forged Ti-6Al-4V alloy.

ACKNOWLEDGEMENTS

This work was supported by the National Natural Science Foundation of China (Grant Nos.51575541, 51711530231).

REFERENCES

[1] Hong SY, Markus I, Jeong W. New cooling approach and tool life improvement in cryogenic machining of titanium alloy

Ti-6Al-4V. *International Journal of Machine Tools and Manufacture* 2001;41(15):2245-2260.

[2] Tan X, Kok Y, Tan YJ, Descoins M, Mangelinck D, Tor SB, Leong KF, Chua CK. Graded microstructure and mechanical properties of additive manufactured Ti-6Al-4V via electron beam melting. *Acta Materialia* 2015;97:1-16.

[3] Chen S, Xu Y, Jiao Y. A hybrid finite-element and cellular-automaton framework for modeling 3D microstructure of Ti-6Al-4V alloy during solid-solid phase transformation in additive manufacturing[J]. *Modelling and Simulation in Materials Science and Engineering*, 2018, 26(4): 045011.

[4] Hu P, Turner JA. Contribution of double scattering in diffuse ultrasonic backscatter measurements. *The Journal of the Acoustical Society of America* 2015;137(1):321-334.

[5] Ghoshal G, Turner JA. Diffuse ultrasonic backscatter at normal incidence through a curved interface. *The Journal of the Acoustical Society of America* 2010;128(6): 3449-3458.

[6] Du H, Lonsdale C, Oliver J, Wilson BM, Turner JA. Evaluation of railroad wheel steel with lamellar duplex microstructures using diffuse ultrasonic backscatter. *Journal of Nondestructive Evaluation* 2013;32(4):331-340.

[8] S. Ahmed and R.B. Thompson: *Review of Progress in Quantitative NDE*, Plenum Press, New York, NY, 1994, vol. 14, pp. 1617-24.

[7] Stanke, F. E. (1986). Spatial autocorrelation functions for calculations of effective propagation constants in polycrystalline materials. *The Journal of the Acoustical Society of America*, 80(5), 1479-1485.